ACS APPLIED MATERIALS & INTERFACES

Research Article

www.acsami.org

Calcium Plasma Implanted Titanium Surface with Hierarchical Microstructure for Improving the Bone Formation

Mengqi Cheng,[†] Yuqin Qiao,[‡] Qi Wang,[†] Guodong Jin,[‡] Hui Qin,[†] Yaochao Zhao,[†] Xiaochun Peng,[†] Xianlong Zhang,*[,†] and Xuanyong Liu*[,‡]

[†]Department of Orthopedics, Shanghai Sixth People's Hospital, Shanghai Jiao Tong University, Shanghai 200233, China

[‡]State Key Laboratory of High Performance Ceramics and Superfine Microstructure, Shanghai Institute of Ceramics, Chinese Academy of Sciences, Shanghai 200050, China

ABSTRACT: Introducing hierarchical microstructure and bioactive trace elements simultaneously onto the surface of titanium implant is a very effective way to improve the osseointegration between bone and implant. In this work, hierarchical topography was prepared on Ti surface via acid etching and sandblasting (SLA) to form micropits and microcavities then underwent Ca plasma immersion ion implantation (Ca–PIII) process. The surface wettability and roughness did not change obviously before and after Ca–PIII process. The in vitro evaluations including cell adhesion, activity, alkaline phosphatase (ALP), osteogenic genes (Runx2, OSX, ALP, BSP, Col1a1, OPN, and OC), and protein (BSP, Col1a1, OPN, and OC) expressions revealed that the introduction of Ca ions onto the surface of SLA-treated Ti can promote greater osteoblasts adhesion, spread and proliferation, which in return further accelerated the maturation and mineralization of osteoblasts. More importantly, in vivo evaluations including Micro-CT evaluation, histological observations, push-out test, sequential fluorescent labeling and histological observations verified that Ca-SLA-treated Ti implants could efficiently promote new bone formation in early times. These promising results suggest that Ca-SLA-treated Ti has the potential for future application in orthopedic field.

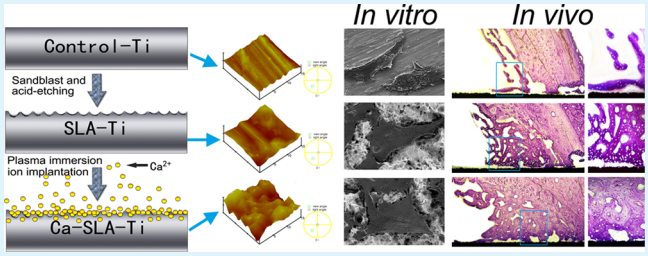

KEYWORDS: *titanium, plasma immersion ion implantation, calcium, SLA, osteogenic activity, osseointegration*

1. INTRODUCTION

Titanium and its alloys are extensively used for fabricating some dental and hip-joint replacement devices because of their favorable mechanical properties and excellent biological performance in bone.[1,2] It is important to know that a rapidly established, strong and long lasting bond at the implant-bone interface is essential for the successful clinical application of implants. Nevertheless, titanium has undesirable failure rates because of its originally limited osseointegration and osteoconductive properties,[3,4] especially in patients who are compromised by disease or age.[5−7] Therefore, direct efforts have been made to optimize the surface characteristics to improve osseointegration for biomaterials. Surface with hierarchical topography at the micrometer scale induced by acid etching and sandblasting (SLA), have been used effectively to enhance the cellular response in vitro[8,9] and the bone formation ability in vivo.[10] For instance, Lee et al. demonstrated that etched microgrooves and ridges were superior to smooth surfaces in inducing differential genes and protein expression of both human bone marrow-derived mesenchymal stem cells (MSCs) and human periodontal ligament cells (PLCs).[11] Many in vivo level studies have also shown that the bone-to-implant contact and removal torque forces were significantly increased.[10,12,13] However, other studies confirmed that the initial cell responses to the microstructure, monitored by cell adhesion and proliferation, were not ideal.[8,14]

Additionally, surface chemistry is also a pivotal factor in the regulation of the interactions between the biomaterial and cells/tissue. Calcium (Ca), magnesium (Mg), zinc (Zn), and other bioactive trace elements have been utilized through different techniques and their beneficial effects on the improvement of biological performance of implant have been proved.[15−19] One technique for modifying the chemical composition of the surface is plasma immersion ion implantation (PIII), a process by which ions are injected into the surface region of a substrate without changing the surface morphology.[20] Previous studies have demonstrated that Ca-implanted titanium forms a suitable biomaterial for cell adhesion, spreading, and proliferation of osteoblasts,[21−23] Furthermore, Ca has also been reported to up-regulate the expression of bone-related genes.[15,24] However, regardless of previous researches that conducted to examine how cells respond to Ca-implanted titanium surface, a comprehensive evaluation of Ca ion implantation on SLA-treated titanium

Received: April 14, 2015
Accepted: May 28, 2015
Published: May 28, 2015

DOI: 10.1021/acsami.5b03209
ACS Appl. Mater. Interfaces 2015, 7, 13053−13061

Table 1. Real-Time Polymerase Chain Reaction Primers Used in This Study

gene	accession number	primers (F, forward; R, reverse)	product size (bp)
β-actin	NM_001101.3	F: CCCAAGGCCAACCGCGAGAAGATG	219
		R: GTCCCGGCCAGCCAGGTCCAGA	
BSP	NM_004967.3	F: AAGAAGGGGAAGAAGAAAGTGTCA	218
		R: GTATTCATTGGCGCCCGTGTATTC	
OSX	NM_001173467.1	F: GCTGCCCACCTACCCATCTGACTT	207
		R: CTGCCCCCATATCCACCACTACCC	
OPN	NM_001040058.1	F: TCTGATGAATCTGATGAACTGGTC	195
		R: GGTGATGTCCTCGTCTGTAGCA	
Col 1a1	NM_000088.3	F: ACCTCCGGCTCCTGCTCCTCTTAG	235
		R: GCGCCGGGGCAGTTCTTGGTCT	
ALP	NM_014476.5	F: GACAATCGGAATGAGCCCACAC	222
		R: GTACTTATCCCGCGCCTTCACCAC	
Runx2	NM_001024630.3	F: TGCGGCCGCCCCACGACAA	200
		R: ACCCGCCATGACAGTAACCACAGT	
OC	NM_199173.4	F: AGCCCAGCGGTGCAGAGTCCA	224
		R: GCCGTAGAAGCGCCGATAGG	

surface on the cell response in vitro and the osseointegration in vivo has not been reported so far.

In this Research Article, hierarchical topography was prepared on Ti surface via SLA to form micropits and microcavities then underwent Ca PIII process. The synergistic effects of hierarchical topography and Ca ions on human osteoblast-like cell line MG63 were evaluated by in vitro cell culture test. In addition, the osseointegration in rabbit model was investigated in vivo. A complete evaluation of the reciprocities at the interface between biomaterial and cells/tissues that involves cell behavior, biomechanical and in vivo osteogenesis assessment will provide more detailed information to understand the biological effects of Ca ion implantation on the SLA-treated Ti surfaces.

2. MATERIALS AND METHODS

2.1. Sample Preparation and Characterization. Commercially pure Ti samples ($\Phi 3 \times 5$ mm^2 and $\Phi 13 \times 2$ mm^2) were ground with SiC paper progressively up to 1200 grits and then ultrasonically cleaned with acetone, ethanol, and distilled water, which is denoted as Control-Ti in this work. After it was dried, the hierarchical microstructure titanium obtained by surface blasting with large particles of aluminum oxide followed by etching and cleaning with HCl/H_2SO_4 (water bath, 8 h, 60 °C), which is denoted as SLA-Ti in this work. The resulting SLA-Ti samples were subjected to calcium ion implantation (denoted as Ca-SLA-Ti in this work) on a multipurpose plasma immersion ion implanter equipped with a calcium arc source for 2 h at a pulse voltage of 15 kV, pulse duration of 500 μs and pulsing frequency of 5 Hz.

Field-emission scanning electron microscopy (FESEM, FEINOVA NanoSEM) was employed to observe the surface topography of the prepared specimens. The surface chemical compositions and depth profiles were determined by X-ray photoelectron spectroscopy (XPS, Physical electronics PHI1800) using Al Ka irradiation at an estimated sputtering rate of 8 nm per minute. Atomic force microscopy (AFM, Nanoscope 3; Bruker, Germany) was used to observe the surface morphology of different samples and the contact angle was determined on a video contact-angle measurement instrument.

2.2. In Vitro Studies. *2.2.1. Cell Culture.* The human MG63 osteoblasts were cultured in Dulbecco's modified Eagle's medium (DMEM, Gibco) containing 10% fetal bovine serum (Gibco) and 1% penicillin/streptomycin at 37 °C in a humidified atmosphere of 5% CO_2. The culture medium was exchanged every 48 h.

2.2.2. Cell Adhesion. MG63 cells (1×10^4 cells/well) were seeded on different samples. After the cells were cultured for 4 and 24 h, each sample was rinsed with phosphate-buffered saline (PBS) for three times to remove the nonadherent cells, then fixed with 95% alcohol and stained with 4′,6′-diamidino-2-phenylindole (DAPI). The cell number was determined in five random fields under an inverted fluorescence microscope (Leica DM400).

2.2.3. Cell Morphology. For cell morphology and cell-material interaction study, MG-63 cells (1×10^4 cells/well) were cultured on different samples. After 1 and 3 days of incubation, the samples were washed with PBS, and fixed with 2.5% glutaraldehyde at 4 °C for 2 h. The further dehydration was conducted with different concentrations of ethanol (50−100%) for 10 min each. Finally, the samples were sputtered coated with gold and observed with field emission scanning electron microscope (FESEM, FEINOVA NanoSEM).

2.2.4. Cell Proliferation Assay. MG-63 cells (1×10^4 cells/well) were seeded onto different samples. After culturing cells for 1, 3, 7, and 14 d, 20 μL of CCK-8 solution and 180 μL of culture medium were added to each well, and then further incubated for 2 h. Finally, the absorbance of the incubated solution was measured by a microplate reader at 450 nm wavelength.

2.2.5. Cell Viability Assay. The viability of cells on control−Ti, SLA−Ti, and Ca−SLA−Ti surfaces was observed by live/dead staining. Briefly, MG-63 cells (1×10^5 cells/well) were seeded on the surface of each sample. After 1 and 3 days of incubation, the seeded samples were washed three times with sterile PBS and then stained with a live/dead Kit (Invitrogen) for 30 min. Cell viability on different samples was evaluated under a fluorescence microscope (Leica DM400).

2.2.6. Alkaline Phosphatase (ALP) Activity Assay. The differentiation behavior of MG63 cells was measured by ALP quantitative assay. MG63 cells (1×10^5 cells/well) were seeded on the samples. After 7, 14, and 21 days of incubation, the cells on different samples were lysed in 0.1% Triton X-100, and then incubated with *p*-nitrophenyl phosphate (*p*NPP) (Sigma) for 60 min at 37 °C. After the reaction was stopped by 1 M NaOH solution, the quantity of *p*-nitrophenol produced was measured at 405 nm and the total protein content was acquired with the aid of a BCA Protein Assay Kit (Sigma).

2.2.7. Real-Time Polymerase Chain Reaction. The expressions of OSX, ALP, Runx2, Col1a1, BSP, OPN, and OC were analyzed by the real-time reverse-transcriptase polymerase chain reaction (real-time RT-PCR). The forward and reverse primers used in this study are listed in Table 1, and the β-actin was used as the internal control gene. After 7 and 14 d of incubation, the total RNA of cells on different samples was extracted using TRIzol reagent (Invitrogen). Subsequently, the complementary DNA (cDNA) was synthesized from 2 μg of total RNA using Reverse Transcriptase M-MLV (Takara). Quantifications of the selected genes were performed using real-time PCR with SYBR Premix Ex Taq (Takara).

2.2.8. Western Blotting Analysis. After MG63 cells were cultured on the different substrates for 7 and 14 days, the total proteins were

DOI: 10.1021/acsami.5b03209
ACS Appl. Mater. Interfaces 2015, 7, 13053−13061

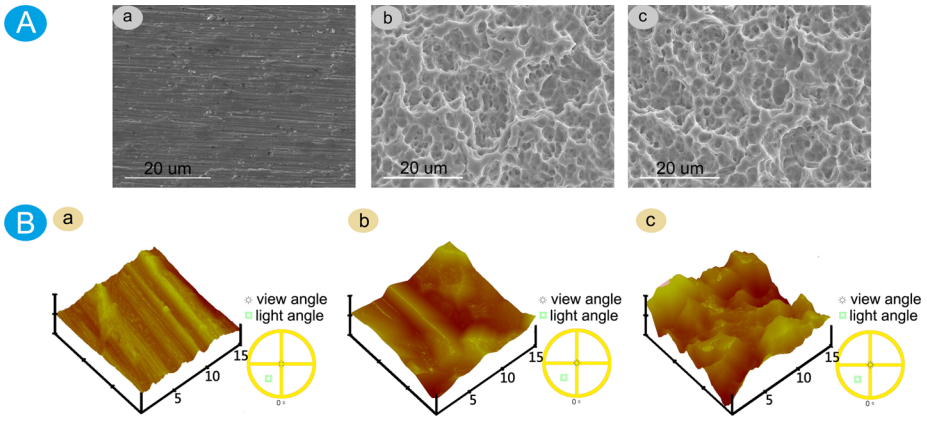

Figure 1. SEM and AFM images of different substrates: (a) control−Ti, (b) SLA−Ti, and (c) Ca−SLA−Ti.

extracted by M-PER Protein Extraction Reagent, and the protein concentration was determined with a BCA protein assay kit (Pierce). Protein extract samples (20 μg) were separated by 10% SDS-PAGE then transferred to polyvinylidene fluoride membranes. After blocking with 5% skim milk for 1 h, the membranes were incubated with different primary antibodies against BSP,OC,OPN and Col1a1 (Santa Cruz Biotechnology, USA) overnight at 4 °C. The membranes were incubated for 1 h with HRP-labeled secondary antibodies (Santa Cruz Biotechnology, USA) and were detected using ECL kit (Pierce).

2.3. In Vivo Animal Studies. *2.3.1. Surgical Procedures.* The animal experiments were approved by the Animal Care Committee of Shanghai Sixth Hospital. Twenty-four adult male New Zealand white rabbits weighting about 2.5−3.0 kg were used in the surgery. All the rabbits were randomly assigned to three groups corresponding to SLA−Ti, Ca−SLA−Ti, and control−Ti. After general anesthesia via intravenous injection of pentobarbital (25 mg/kg), the surgical site was sterilized with iodophor disinfectant. Then two holes with a diameter of 3.0 mm were drilled on the midshaft of femurs using a hand drill until exposure to marrow. Afterward the bone cavities were swilled with physiological saline, and the implants were pressed into the prepared holes (Figure 8a). To reduce the peri-operative infection risk, oxytetracycline (30 mg/kg) and ketoprofen (3 mg/kg) were injected postoperatively for 3 consecutive days. The new bone formed was double labeled by alizarin red (30 mg/kg) and calcein (20 mg/kg) (Sigma), which were intraperitoneally injected at 4 and 8 weeks, respectively, after the operation.

2.3.2. Push-Out Test. The push-out test was implemented on a biomechanical test device (Instron 5569 electromechanical testing system, Instron, Canton, MA). Four femur samples in each group were harvested 12 weeks postoperation and fixed on a steel device with bone cement (Figure 8b). The tests were performed at a loading rate of 1 mm/min. The load-deflection curves were recorded during the pushing period and the failure load was defined as the maximum load values.

2.3.3. Micro-CT Evaluation. Four femur samples with implants in each group were underwent microcomputed tomography (Micro-CT) evaluation in a microcomputerized tomography (micro-CT) setup (SKYSCAN 1176, Bruker). After they were scanned, the two-dimensional (2D) images were obtained immediately and the three-dimensional (3D) models were reconstructed with a CTVol program (Skyscan Company). Furthermore, the new bone volume and trabecular thickness within the scope of 1 mm in diameter around implants were determined by the CTAn program (Skyscan Company).

2.3.4. Histological Evaluation. Four femur samples with implants in each group were fixed in acetone for 1 week, dehydrated in a series of alcohol solutions from 75% to 100%, and embedded in methyl methacrylate without decalcification. Then the nondecalcified sections were made on a saw microtome (Leica SP1600) and subsequently polished to about 50 μm in thickness for fluorochrome markers observation using a confocal laser scanning microscope (CLSM, Leica). Finally, the nondecalcified sections were stained with 1% methylene blue, and observed under a Leica microscope (Leica DM400). The bone-to-implant contact (BIC) values were calculated.

2.4. Statistical Analysis. All the in vitro experiments were independently performed in triplicates and each data point represents three replicate measurements. The data were expressed as averages ± standard deviations. The results of the in vitro and in vivo experiments were statistically analyzed by the one-way analysis of variance (ANOVA) and a p value less than 0.05 was considered to be statistically significant.

3. RESULTS AND DISCUSSION

3.1. Characterization of Samples. SEM images of Control-Ti, SLA-Ti and Ca-SLA-Ti surfaces are shown in Figure 1A. Some minor scratches, stemming from the polishing treatments, were clearly seen on the Control-Ti surface (Figure 1Aa). Nevertheless, both SLA-Ti and Ca-SLA-Ti displayed tremendous rough surfaces with small micro pits and sharp edges, indicating that without any visible changes before and after Ca ion implantation (Figure 1Ab and 1Ac). The qualitative increased roughness of the Ti surface detected by electron microscopy after the SLA treatment was confirmed by AFM analyses (Figure 1B). As expected, average roughness measurements revealed that the microroughness of the SLA-Ti and Ca-SLA-Ti was significantly higher than for the Control-Ti (Table 2). However, there is no big difference between SLA-Ti and Ca-SLA-Ti in average roughness, corresponding to the previous studies.[22]

Table 2. Comparison among Control−Ti, SLA−Ti, and Ca−SLA−Ti in Terms of Surface Roughness and Contact Angle

	R_a (μm)	contact angle (deg)
control−Ti	0.19 ± 0.22	74.04 ± 8.86
SLA−Ti	1.21 ± 0.52	119.81 ± 2.53
Ca−SLA−Ti	1.15 ± 0.78	111.71 ± 4.18

The surface wettability of different samples was characterized by the water contact angles. As shown in Table 2, control−Ti substrates displayed contact angle of 74.04 ± 8.86°. SLA−Ti substrates showed hydrophobicity with contact angle of 119.81 ± 2.53°, while the contact angle of Ca−SLA−Ti was 111.71 ± 4.18°. Our results revealed that the surface wettability before and after Ca−PIII does not change significantly, and so the effect of surface wettability on the in vitro cytocompatibility can be neglected.

The XPS full spectrum acquired from Ca-SLA-Ti surfaces is displayed in Figure 2a. It can be observed that titanium,

DOI: 10.1021/acsami.5b03209
ACS Appl. Mater. Interfaces 2015, 7, 13053−13061

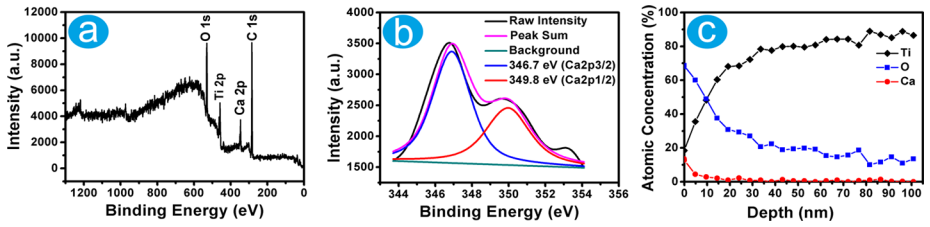

Figure 2. (a) Wide-scan survey spectra, (b) high-resolution XPS spectra, and (c) depth profile acquired from the Ca−SLA−Ti.

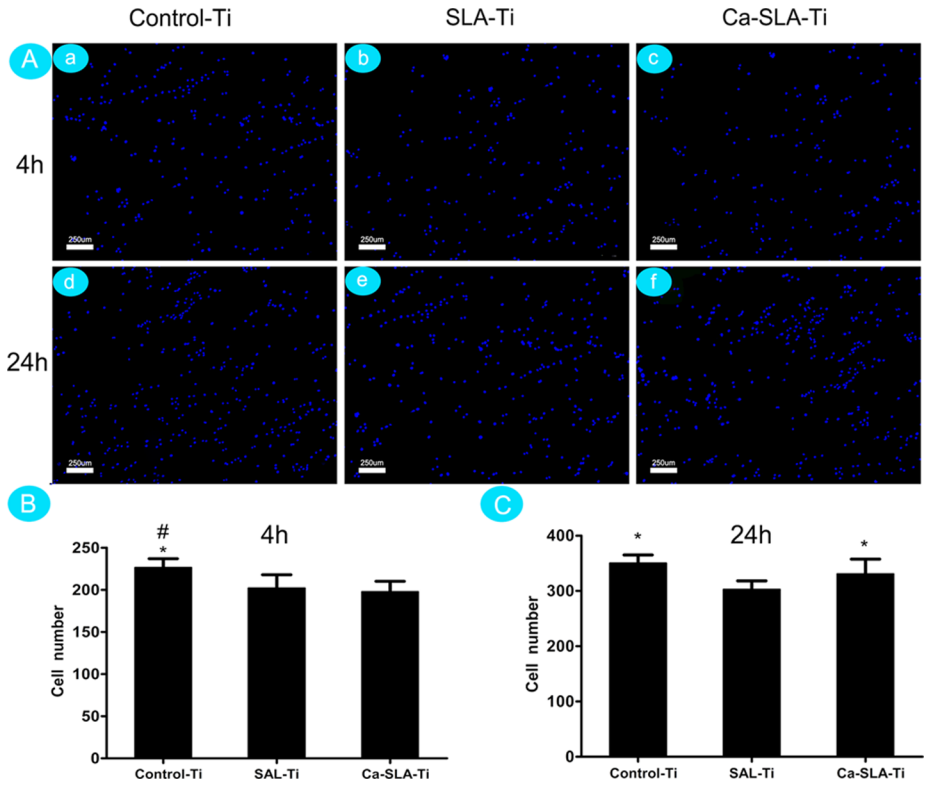

Figure 3. Adhesion of MG63 cells on the samples as determined by counting the cells stained with the DAPI under a fluorescence microscope after incubation for (B) 4 and (C) 24 h: (a, d) control−Ti, (b, e) SLA−Ti, (c, f) Ca−SLA−Ti; *p < 0.05 compared to the SLA−Ti, #p < 0.05 compared to the Ca−SLA−Ti.

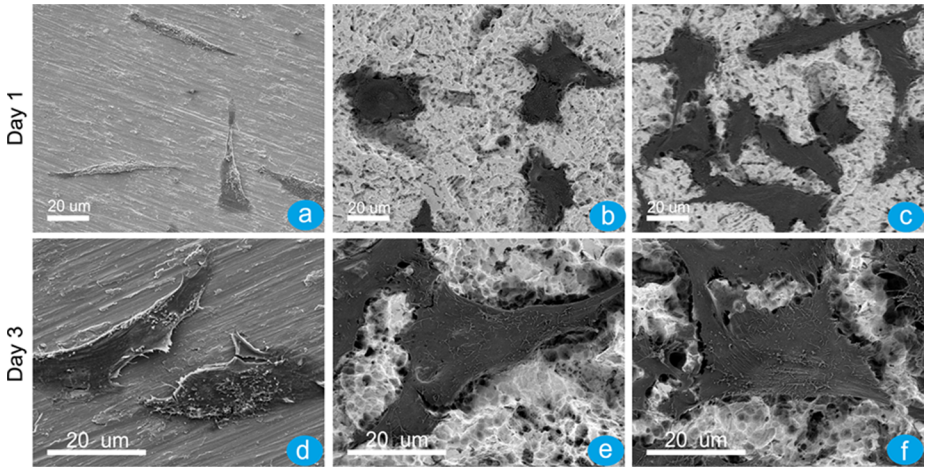

Figure 4. Cell morphology on the samples after 1 and 3 days of incubation displayed by SEM: (a, d) control−Ti, (b, e) SLA−Ti, and (c, f) Ca−SLA−Ti.

calcium, oxygen and carbon elements were detected on the surfaces. The Ca 2p spectrum shown in Figure 2b exhibited double peaks at about 346.7 (2p 3/2) and 349.8 eV (2p 1/2), suggesting the existence of $Ca(OH)_2$ or CaO.[25] The XPS depth

DOI: 10.1021/acsami.5b03209
ACS Appl. Mater. Interfaces 2015, 7, 13053−13061

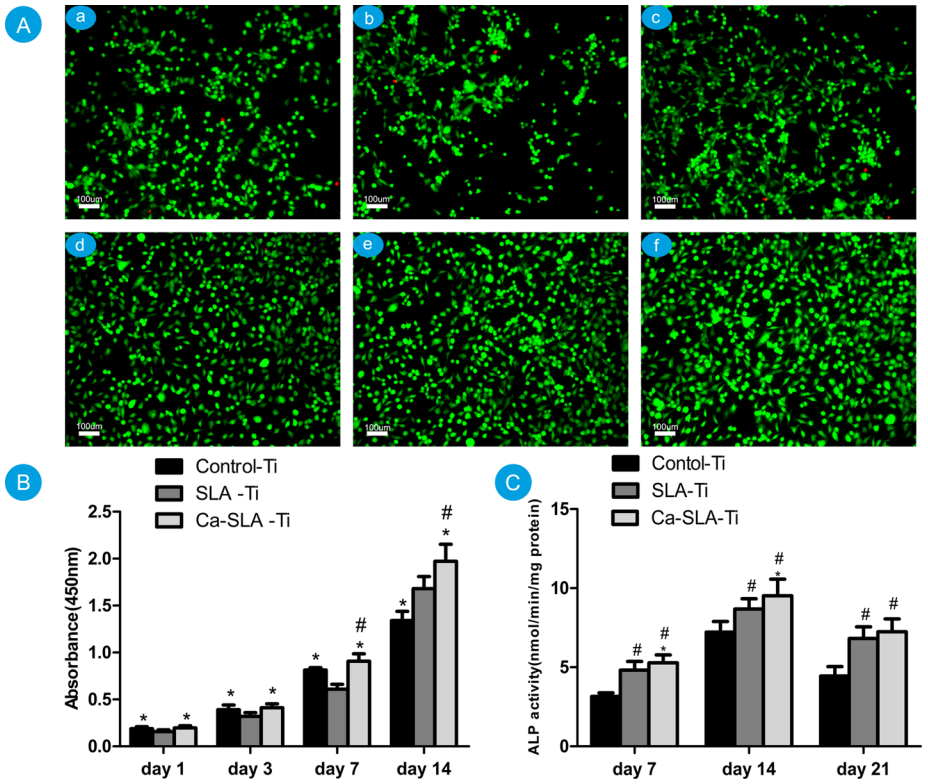

Figure 5. (A) Viability of osteoblast on different samples using live/dead assay with fluorescence microscope of day 1 and 3 culture: (a, d) viability on control−Ti, (b, e) SLA−Ti, and (c, f) Ca−SLA−Ti, respectively. Live cells produced green fluorescence and dead cells red fluorescence. (B) CCK-8 assay of osteoblast cells cultured for 1, 3, 7, and 14 days on different Ti substrates. (C) Alkaline phosphatase activity of osteoblasts adhered to different Ti substrates after culture for 7, 14, and 21 days, respectively. *$p < 0.05$ compared to the SLA−Ti, #$p < 0.05$ compared to the Ca−SLA−Ti.

profile of Ca−SLA−Ti is shown in Figure 2c. It can be seen that a CaO layer about 18 nm thick was formed on the Ca−SLA−Ti surface after ion implantation, and the highest atomic concentration of Ca and O was found on the outermost surface of total depth.

3.2. In Vitro Osteoblast Response Evaluation. Cell adhesion belongs to the first phase of cell/material interactions, which highly regulate the following cell proliferation, migration and differentiation.[26−28] The cell adhesion behavior was evaluated via DAPI staining (Figure 3). Quantitative determination of cells binding to the different substrates showed that the cells on the SLA−Ti and Ca−SLA−Ti substrates were significantly reduced at 4 h compared with the control−Ti, which may be attributed to the hydrophobicity of the SLA−Ti and Ca−SLA−Ti.[29] However, after 24 h incubation, the number of cells adhering to the control−Ti and Ca−SLA−Ti substrates was significantly higher than SLA−Ti. Since the roughness and contact angle of the SLA−Ti surface were not significantly altered by Ca ions implantation, we suggested that the effects observed in the present study were due to the Ca ions.

Meanwhile, SEM analysis was performed after 1 and 3 d, respectively. Figure 4 demonstrates the interactions between the cells and the surfaces. After 1 day of cultivation, slender or spherical cells with a slight extracellular membrane bridge can be seen on the surfaces of control−Ti and SLA−Ti. However, cells on the surface of Ca−SLA−Ti presented a wide cellular membrane bridge and flattened morphology. Furthermore, after 3 days of cultivation, cells incubated on the Ca-SLA-Ti samples were found to be more flattened and presented more filopodia extending from the leading edges compared with those on the control−Ti and SLA−Ti samples, suggesting that the metabolism and synthetic activity of the osteoblasts may be relatively enhanced by the Ca ion implantation.[30]

The cell viability was evaluated by live/dead staining. The result showed that nearly all cells were viable during cultivation on each sample, and cell density on Ca−SLA−Ti surface was higher among all samples, indicating that the good cell viability after Ca ion implantation (Figure 5A). In addition, cell proliferation measured by the CCK-8 assay is shown in Figure 5B. It could be found that osteoblasts on different samples all proliferated as time went on, and osteoblasts adhered to SLA−Ti sample grew not so well as other groups after culture for 1, 3, and 7 days. However, after Ca implantation, significantly increased cell proliferation can be observed on Ca−SLA−Ti at each time point compared to SLA−Ti, revealing that Ca implantation into SLA−Ti offers a more favorable cell environment for cell proliferation. The results of that CCK-8 assay are consistent with those of other studies that reported the beneficial effects of Ca ions in cell proliferation.[31] The results of ALP assay are shown in Figure 5C. ALP activity increased as culture time went on, and the Ca−SLA−Ti surface showed significantly higher ALP activity than control−Ti and SLA−Ti surfaces after culture for 7 and 14 d. After 21 d of culture, ALP activity decreased compared with 14 d of culture, as ALP is an important marker of early differentiation period.

The differentiation of MG63 cells on the control−Ti, SLA−Ti, and Ca−SAL−Ti surface can be estimated in terms of the mRNA expressions of ALP, Runx2, OSX, OPN, OC, and Col1a1. ALP is commonly employed to be an early marker for osteogenic differentiation.[32,33] Our results revealed that the ALP mRNA expression of MG63 cells on the Ca-SLA-Ti

DOI: 10.1021/acsami.5b03209
ACS Appl. Mater. Interfaces 2015, 7, 13053−13061

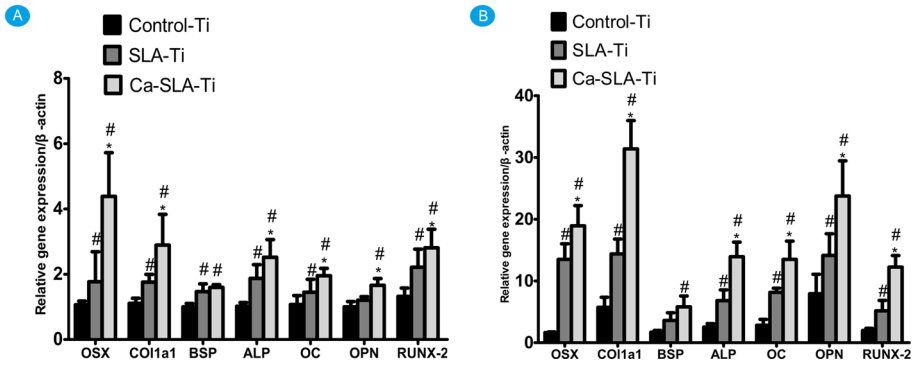

Figure 6. Osteogenic differentiation by measuring the mRNA expression level of Osterix (OSX), alpha-1 type I collagen (Col1a1), bone sialoprotein (BSP), alkaline phosphatase (ALP), osteocalcin (OC), osteopontin (OPN) and runt-related transcription factor 2 (Runx2) after (A) 7 d and (B) 14 d. The value was normalized to *β*-actin. Error bars represent mean ± SD for $n = 3$, #$p < 0.05$ compared to the Control−Ti, and *$p < 0.05$ compared to the SLA−Ti.

surface was significantly higher than those on the control−Ti and SLA−Ti surfaces at 7 and 14 days (Figure 6A, B). Runx2 is known to be an osteoblast-specific transcription factor that is essential for differentiation of osteoblasts and can activate the expressions of downstream osteogenic genes, such as ALP, Col1a1, OC, and OPN.[34,35] OSX, containing a zinc finger, is considered to be a crucial role in inducing the maturation of osteoblasts.[36] In this study, the expression of Runx2 and OSX mRNAs were higher on the Ca−SLA−Ti surface when compared to the control−Ti and SLA−Ti surfaces (Figure 6A, B). These results demonstrate that the Ca ion implantation can accelerate the osteoblasts differentiation, which is further confirmed by the genes and proteins expression of OPN, OC, and Col1a1 (Figures 6 and 7). Col1a1 is one of the major

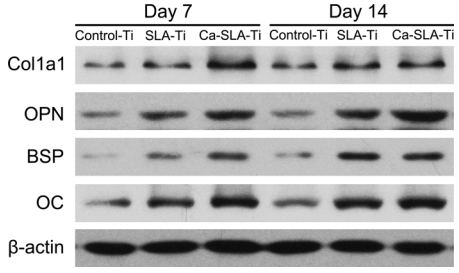

Figure 7. Effects of control−Ti, SLA−Ti, and Ca−SLA−Ti on the protein expression of Col1a1, OPN, BSP, and OC.

components of extra cellular matrix deposition. The early and higher expression of Col1a1 at both gene and protein levels suggested that Ca−SLA−Ti surface can induce osteoblastic differentiation.[37] OPN plays a major role in the early differentiation of osteoblasts and at the initial stage of biomineralization by osteoblasts in bone.[38] OC is a late-stage maker of osteoblast differentiation and its production denotes the onset of ECM deposition.[39,40] In this work, OPN and OC showed a significant higher expression at both gene and protein levels on Ca−SLA−Ti surface compared to control at day 7 and 14. Taking the upper results together, we believe that the Ca−SLA−Ti surface not only can promote the cell maturation but also can facilitate ECM mineralization at an earlier time. For BSP, although the up-regulation was also observed on the Ca−SLA−Ti surface, there were no significant differences between SLA−Ti and Ca−SLA−Ti at both gene and protein levels.

3.3. In Vivo Osseointegration Studies. To investigate the impact of microstructure and calcium ions on osseointegration in vivo, as shown in Figure 8a, we prepared cylindrical rods and implanted into femoral of New Zealand rabbit. After 12 weeks, push-out experiments (Figure 8b) were performed to analyze the interfacial binding capacity between implants and bone tissues. The typical load-deflection curves and average push-out loads are shown in Figure 8c−f. The average maximum push-out loads obtained from control−Ti, SLA−Ti, and Ca−SLA−Ti are 35.4, 60.5, and 86.2 N, respectively. It is obvious that materials with Ca−SLA surfaces have higher bonding strength than the controls, suggesting a high level of mechanical interlocking between the implant and bones.

New bone formation around implants surface in the bone marrow cavity after operation were evaluated at prescribed time points by micro-CT. Figure 9A shows the coronal sections of the femur containing the implants 4, 8, and 12 weeks after surgery. As seen from the two-dimensional images, it could be found that the new bone formation (red triangle) surrounding all implants increased along with the implantation time past. The quantitative assessments of new bone volume (NB) and trabecular thickness (TH) were determined in a sequence of Ca−SLA−Ti > SLA−Ti > control−Ti (Figures 9B, C). Furthermore, there was more new bone formed around SLA−Ti than that of control−Ti.

The new bone formation and mineralization process around implants was observed by two types of fluorochrome labeling at specific time intervals of 4 and 8 weeks (Figure 10). After 4 weeks, Stronger density and more widely spread area of Alizarin Red S fluorescence (red) were observed around the Ca−SLA−Ti surface than the others, which demonstrated that newly formed bone tissues grew much more energetically around Ca−SLA−Ti implant than around control−Ti and SLA−Ti implants. At a later time point (8 weeks), calcein (green) is incorporated into the bone closest to the implant coatings demonstrating similar patterns. In general, sequential fluorescent labeling shows that Ca−SLA−Ti stimulates more new bone formation, especially at the early time point (4 weeks). The early bone response to implants is critical for the degree of bone to implant contact and subsequently for implant fixation, which may be explained by the early stimulation of bone healing at the implant interface by the applied Ca ions.

To evaluate the bone regenerating capacity of the Ca−SLA−Ti surface, Histological stained sections stained with toluidine blue are shown in Figure 11A. In the cortico-cancellous site,

DOI: 10.1021/acsami.5b03209
ACS Appl. Mater. Interfaces 2015, 7, 13053−13061

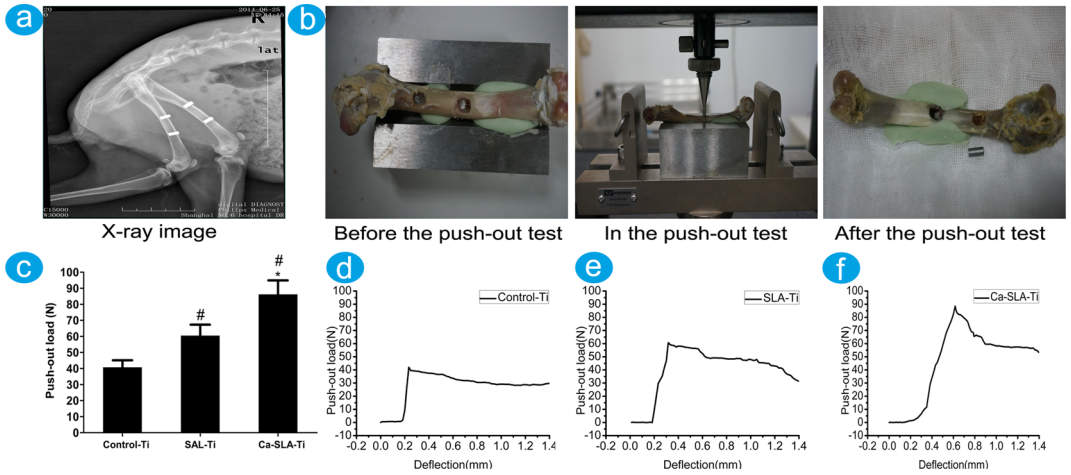

Figure 8. Surgical and push-out test: (a) X-ray observation illustrating the in vivo process, (b) the process of push out test, and (c) average maximum push-out load of the implants. Error bars represent mean ± SD for $n = 4$, #$p < 0.05$ compared to the control−Ti, and *$p < 0.05$ compared to the SLA−Ti. Load-deflection curves of (d) control−Ti, (e) SLA−Ti, and (f) Ca−SLA−Ti implants.

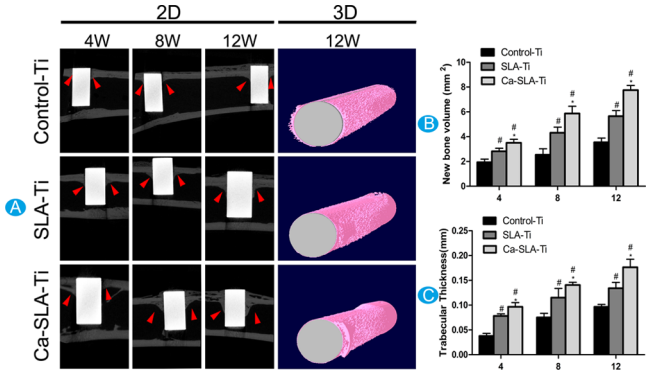

Figure 9. Characterization of implants and the surrounding bones by Micro-CT: (A) Micro-CT 2D (The red triangles refer to the newly formed bone) and 3D reconstruction models showing the status of the implants (white in color) and bone (pink in color) response 4, 8, and 12 weeks after surgery; (B) quantitative analysis of new bone volume and (C) trabecular thickness. Error bars represent mean ± SD for $n = 4$, #$p < 0.05$ compared to the control−Ti, and *$p < 0.05$ compared to the SLA−Ti.

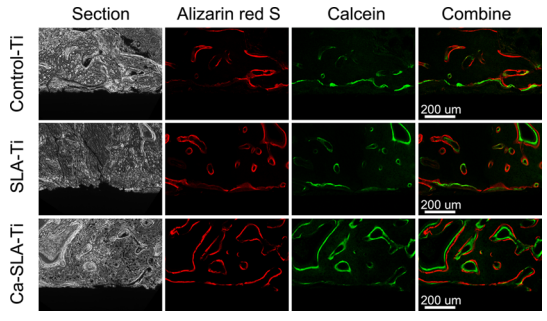

Figure 10. Sequential polychrome labels observed for 12 weeks in rabbit models: alizarin red S (red, 4 weeks) and calcein (green, 8 weeks).

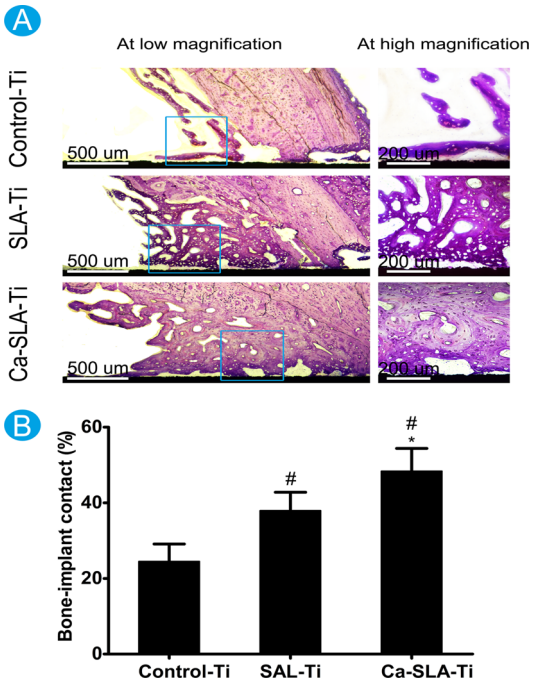

Figure 11. (A) Toluidine blue staining images and (B) the bone-implant contact values of control−Ti, SLA−Ti, and Ca−SLA−Ti after implantation for 12 weeks. Error bars represent mean ± SD for $n = 4$, #$p < 0.05$ compared to the control−Ti, and *$p < 0.05$ compared to the SLA−Ti.

only small amount of loose trabecular bone was found at the interfaces of Ti−bone, whereas relatively compact newly formed trabecular bone was observed at the both interfaces of SLA−Ti/bone and Ca−SLA−Ti/bone. At the same time, From the high magnification images, we could also observe that the area and thickness of the trabecular were strongly increased after Ca implantation. Furthermore, as shown in Figure 11B, the bone-implant contact (BIC) value for Ca−SLA−Ti implants was significantly higher than the other groups. Taking into account of the Micro-CT results, it is reasonable to believe that the incorporation of Ca ions on the rough surface can improve the in vivo osseointegration.

As is known to all, the process of bone formation includes cell adhesion, spread, proliferation, differentiation, mineralization, which is regulated by the surface topography and elemental composition of materials. Microtextured topography has been shown that could induce osteogenesis-related genes express to increase osteoblastic differentiation. However, K. Anselme and other researchers also found that cell adhesion

DOI: 10.1021/acsami.5b03209
ACS Appl. Mater. Interfaces 2015, 7, 13053−13061

and proliferation decreased with increasing material surface roughness.[8,14,41] To tackle this problem, we introduced the calcium ions on the surface of SLA−Ti in this study. Osteoblasts grown on Ca−SLA−Ti surfaces exhibited significantly better cell adhesion, spread and proliferation than that of cells on SLA−Ti surfaces, which is somewhat in accordance with recently reported studies on Ca-incorporated Ti surfaces.[21,23] Nayab et al. also found that integrin, fibronectin, vitronectin and OPN, involved in osteoblast attachment, gene expressions were significantly increased after Ca implantation.[15,21,24,42] Although the exact mechanism is not yet understood, these findings may at least partly explain the enhanced cell adhesion and proliferation we observed in this study. Compared to SLA−Ti, the differentiation-related genes and proteins, especially Col1a1, OPN and OC, were significantly enhanced, suggesting the implantation of Ca ions further promote the differentiation of MG63 cells beyond that of SLA alone. Moreover, the results of in vivo experiments nicely correlate with the above-mentioned in vitro findings. Because the quality of cell adhesion, spreading and proliferation(the early osteoblast response) will influence their capacity for differentiation and mineralization(the later osteoblast response),[26] so it can be inferred that a sufficient Ca component in the outer oxide layer of SLA−Ti enhanced cell attachment and proliferation, which in turn resulted in enhanced bone formation. In addition, the surface microstructure may be another possible reason for enhanced osteoconductivity of Ca−SLA−Ti implants, which might increase the reactivity of Ca implanted surface by enlarging its surface area exposed to the biological environment.[43] To sum up, the combination of hierarchical microstructure and Ca ions can synergistically promoted the bone formation of Ti implants in vitro and in vivo, and the specific mechanism of the Ca ions implantation onto SLA surface in regulating the bone formation process needs further study.

4. CONCLUSION

In summary, our result demonstrated that the introduction of Ca ions onto the surface of SLA−Ti with assistance of plasma immersion ion implantation technique can promote greater osteoblasts adhesion/proliferation, which in return further accelerated the maturation and the mineralization of osteoblasts in vitro, as well as osseointegration in vivo. The potential mechanism was proposed that both microstructure and calcium ions contributed to the improved osseointegration of Ca−SLA−Ti implant. This study provides an alternative for the biofunctionalization of titanium-based implants for orthopedic applications.

AUTHOR INFORMATION

Corresponding Authors

*E-mail: zhangxianl197826@163.com.
*E-mail: xyliu@mail.sic.ac.cn.

Author Contributions

M.C and Y.Q. contributed equally.

Notes

The authors declare no competing financial interest.

ACKNOWLEDGMENTS

Financial support from the National Basic Research Program of China (973 Program, 2012CB933600), National Natural Science Foundation of China (81271962, 81301571, 81201425, 81271704, and 31200721), and Shanghai Committee of Science and Technology, China (12JC1407302 and 14XD1403900), are acknowledged.

REFERENCES

(1) Liu, X.; Chu, P.; Ding, C. Surface Modification of Titanium, Titanium Alloys, and Related Materials for Biomedical Applications. *Mater. Sci. Eng., R* **2004**, *47*, 49−121.
(2) Gil, F. J.; Manzanares, N.; Badet, A.; Aparicio, C.; Ginebra, M. P. Biomimetic Treatment on Dental Implants for Short-Term Bone Regeneration. *Clin. Oral Investig.* **2014**, *18*, 59−66.
(3) Jonasova, L.; Muller, F. A.; Helebrant, A.; Strnad, J.; Greil, P. Biomimetic Apatite Formation on Chemically Treated Titanium. *Biomaterials* **2004**, *25*, 1187−1194.
(4) Nebe, J. B.; Muller, L.; Luthen, F.; Ewald, A.; Bergemann, C.; Conforto, E.; Muller, F. A. Osteoblast Response to Biomimetically Altered Titanium Surfaces. *Acta Biomater.* **2008**, *4*, 1985−1995.
(5) Fransson, C.; Wennstrom, J.; Berglundh, T. Clinical Characteristics at Implants with a History of Progressive Bone Loss. *Clin. Oral Implants Res.* **2008**, *19*, 142−147.
(6) Granstrom, G. Osseointegration in Irradiated Cancer Patients: An Analysis with Respect to Implant Failures. *J. Oral Maxillofac. Surg.* **2005**, *63*, 579−585.
(7) Esposito, M.; Hirsch, J. M.; Lekholm, U.; Thomsen, P. Biological Factors Contributing to Failures of Osseointegrated Oral Implants. (II). Etiopathogenesis. *Eur. J. Oral Sci.* **1998**, *106*, 721−764.
(8) Gittens, R. A.; Olivares-Navarrete, R.; Cheng, A.; Anderson, D. M.; McLachlan, T.; Stephan, I.; Geis-Gerstorfer, J.; Sandhage, K. H.; Fedorov, A. G.; Rupp, F.; Boyan, B. D.; Tannenbaum, R.; Schwartz, Z. The Roles of Titanium Surface Micro/Nanotopography and Wettability on the Differential Response of Human Osteoblast Lineage Cells. *Acta Biomater.* **2013**, *9*, 6268−6277.
(9) Zinger, O.; Zhao, G.; Schwartz, Z.; Simpson, J.; Wieland, M.; Landolt, D.; Boyan, B. Differential Regulation of Osteoblasts by Substrate Microstructural Features. *Biomaterials* **2005**, *26*, 1837−1847.
(10) Cochran, D. L.; Buser, D.; ten Bruggenkate, C. M.; Weingart, D.; Taylor, T. M.; Bernard, J. P.; Peters, F.; Simpson, J. P. The Use of Reduced Healing Times on ITI (R) Implants with a Sandblasted and Acid-etched (SLA) Surface: Early Results from Clinical Trials on ITI (R) SLA Implants. *Clin. Oral Implants Res.* **2002**, *13*, 144−153.
(11) Lee, M. H.; Kang, J. H.; Lee, S. W. The Significance of Differential Expression of Genes and Proteins in Human Primary Cells Caused by Microgrooved Biomaterial Substrata. *Biomaterials* **2012**, *33*, 3216−3234.
(12) Buser, D.; Schenk, R. K.; Steinemann, S.; Fiorellini, J. P.; Fox, C. H.; Stich, H. Influence of Surface Characteristics on Bone Integration of Titanium Implants. A Histomorphometric Study in Miniature Pigs. *J. Biomed. Mater. Res.* **1991**, *25*, 889−902.
(13) Cho, S. A.; Park, K. T. The Removal Torque of Titanium Screw Inserted in Rabbit Tibia Treated by Dual Acid Etching. *Biomaterials* **2003**, *24*, 3611−3617.
(14) Raines, A. L.; Olivares-Navarrete, R.; Wieland, M.; Cochran, D. L.; Schwartz, Z.; Boyan, B. D. Regulation of Angiogenesis During Osseointegration by Titanium Surface Microstructure and Energy. *Biomaterials* **2010**, *31*, 4909−4917.
(15) Nayab, S. N.; Jones, F. H.; Olsen, I. Effects of Calcium Ion-Implantation of Titanium on Bone Cell Function in Vitro. *J. Biomed. Mater. Res., Part A* **2007**, *83*, 296−302.
(16) Kim, B. S.; Kim, J. S.; Park, Y. M.; Choi, B. Y.; Lee, J. Mg Ion Implantation on SLA-Treated Titanium Surface and Its Effects on the Behavior of Mesenchymal Stem Cell. *Mater. Sci. Eng., C* **2013**, *33*, 1554−1560.
(17) Shen, X.; Hu, Y.; Xu, G.; Chen, W.; Xu, K.; Ran, Q.; Ma, P.; Zhang, Y.; Li, J.; Cai, K. Regulation of the Biological Functions of Osteoblasts and Bone Formation by Zn-Incorporated Coating on Microrough Titanium. *ACS Appl. Mater. Interfaces* **2014**, *6*, 16426−16440.

DOI: 10.1021/acsami.5b03209
ACS Appl. Mater. Interfaces 2015, 7, 13053−13061

(18) Qiao, Y.; Zhang, W.; Tian, P.; Meng, F.; Zhu, H.; Jiang, X.; Liu, X.; Chu, P. K. Stimulation of Bone Growth Following Zinc Incorporation into Biomaterials. *Biomaterials* **2014**, *35*, 6882−6897.
(19) Liang, C.; Wang, H.; Yang, J.; Cai, Y.; Hu, X.; Yang, Y.; Li, B.; Li, H.; Li, H.; Li, C.; Yang, X. Femtosecond Laser-Induced Micropattern and Ca/P Deposition on Ti Implant Surface and Its Acceleration on Early Osseointegration. *ACS Appl. Mater. Interfaces* **2013**, *5*, 8179−8186.
(20) Zhao, Y.; Wong, S. M.; Wong, H. M.; Wu, S.; Hu, T.; Yeung, K. W.; Chu, P. K. Effects of Carbon and Nitrogen Plasma Immersion Ion Implantation on in Vitro and in Vivo Biocompatibility of Titanium Alloy. *ACS Appl. Mater. Interfaces* **2013**, *5*, 1510−1516.
(21) Nayab, S. N.; Jones, F. H.; Olsen, I. Effects of Calcium Ion Implantation on Human Bone Cell Interaction with Titanium. *Biomaterials* **2005**, *26*, 4717−4727.
(22) Nayab, S.; Shinawi, L.; Hobkirk, J.; Tate, T. J.; Olsen, I.; Jones, F. H. Adhesion of Bone Cells to Ion-Implanted Titanium. *J. Mater. Sci. Mater. Med.* **2003**, *14*, 991−997.
(23) Nayab, S. N.; Jones, F. H.; Olsen, I. Human Alveolar Bone Cell Adhesion and Growth on Ion-Implanted Titanium. *J. Biomed. Mater. Res., Part A* **2004**, *69*, 651−657.
(24) Sawada, R.; Kono, K.; Isama, K.; Haishima, Y.; Matsuoka, A. Calcium-Incorporated Titanium Surfaces Influence the Osteogenic Differentiation of Human Mesenchymal Stem Cells. *J. Biomed. Mater. Res., Part A* **2013**, *101*, 2573−2585.
(25) Krupa, D.; Baszkiewicz, J.; Kozubowski, J. A.; Barcz, A.; Sobczak, J. W.; Biliniski, A.; Lewandowska-Szumiel, M. D.; Rajchel, B. Effect of Calcium-Ion Implantation on the Corrosion Resistance and Biocompatibility of Titanium. *Biomaterials* **2001**, *22*, 2139−2151.
(26) Anselme, K. Osteoblast Adhesion on Biomaterials. *Biomaterials* **2000**, *21*, 667−681.
(27) Miyauchi, T.; Yamada, M.; Yamamoto, A.; Iwasa, F.; Suzawa, T.; Kamijo, R.; Baba, K.; Ogawa, T. The Enhanced Characteristics of Osteoblast Adhesion to Photofunctionalized Nanoscale TiO_2 Layers on Biomaterials Surfaces. *Biomaterials* **2010**, *31*, 3827−3839.
(28) Derhami, K.; Wolfaardt, J. F.; Wennerberg, A.; Scott, P. G. Quantifying the Adherence of Fibroblasts to Titanium and Its Enhancement by Substrate-Attached Material. *J. Biomed. Mater. Res.* **2000**, *52*, 315−322.
(29) Zhu, X.; Chen, J.; Scheideler, L.; Reichl, R.; Geis-Gerstorfer, J. Effects of Topography and Composition of Titanium Surface Oxides on Osteoblast Responses. *Biomaterials* **2004**, *25*, 4087−4103.
(30) Leitao, E.; Barbosa, M. A.; De Groot, K. In Vitro Testing of Surface-Modified Biomaterials. *J. Mater. Sci. Mater. Med.* **1998**, *9*, 543−548.
(31) Sul, Y. T.; Byon, E. S.; Jeong, Y. Biomechanical Measurements of Calcium-Incorporated Oxidized Implants in Rabbit Bone: Effect of Calcium Surface Chemistry of a Novel Implant. *Clin. Implant Dent. Relat. Res.* **2004**, *6*, 101−110.
(32) Tsigkou, O.; Jones, J. R.; Polak, J. M.; Stevens, M. M. Differentiation of Fetal Osteoblasts and Formation of Mineralized Bone Nodules by 45S5 Bioglass Conditioned Medium in the Absence of Osteogenic Supplements. *Biomaterials* **2009**, *30*, 3542−3550.
(33) Nayak, S.; Dey, T.; Naskar, D.; Kundu, S. C. The Promotion of Osseointegration of Titanium Surfaces by Coating with Silk Protein Sericin. *Biomaterials* **2013**, *34*, 2855−2864.
(34) Komori, T. Regulation of Osteoblast Differentiation by Transcription Factors. *J. Cell. Biochem.* **2006**, *99*, 1233−1239.
(35) Ducy, P.; Karsenty, G. Genetic Control of Cell Differentiation in the Skeleton. *Curr. Opin. Cell Biol.* **1998**, *10*, 614−619.
(36) Nakashima, K.; Zhou, X.; Kunkel, G.; Zhang, Z. P.; Deng, J. M.; Behringer, R. R.; de Crombrugghe, B. The Novel Zinc Finger-Containing Transcription Factor Osterix Is Required for Osteoblast Differentiation and Bone Formation. *Cell* **2002**, *108*, 17−29.
(37) Zhao, Y.; Wong, H. M.; Wang, W.; Li, P.; Xu, Z.; Chong, E. Y.; Yan, C. H.; Yeung, K. W.; Chu, P. K. Cytocompatibility, Osseointegration, and Bioactivity of Three-Dimensional Porous and Nanostructured Network on Polyetheretherketone. *Biomaterials* **2013**, *34*, 9264−9277.
(38) Liu, L.; Qin, C.; Butler, W. T.; Ratner, B. D.; Jiang, S. Controlling the Orientation of Bone Osteopontin via Its Specific Binding with Collagen I to Modulate Osteoblast Adhesion. *J. Biomed. Mater. Res., Part A* **2007**, *80*, 102−110.
(39) Huang, R.; Lu, S.; Han, Y. Role of Grain Size in the Regulation of Osteoblast Response to Ti−25Nb−3Mo−3Zr−2Sn Alloy. *Colloids Surf. B. Biointerfaces* **2013**, *111*, 232−241.
(40) Wang, C. Y.; Duan, Y. R.; Markovic, B.; Barbara, J.; Howlett, C. R.; Zhang, X. D.; Zreiqat, H. Proliferation and Bone-Related Gene Expression of Osteoblasts Grown on Hydroxyapatite Ceramics Sintered at Different Temperature. *Biomaterials* **2004**, *25*, 2949−2956.
(41) Anselme, K.; Bigerelle, M. Topography Effects of Pure Titanium Substrates on Human Osteoblast Long-Term Adhesion. *Acta Biomater.* **2005**, *1*, 211−222.
(42) Schneider, G. B.; Zaharias, R.; Stanford, C. Osteoblast Integrin Adhesion and Signaling Regulate Mineralization. *J. Dent. Res.* **2001**, *80*, 1540−1544.
(43) Park, J. W.; Park, K. B.; Suh, J. Y. Effects of Calcium Ion Incorporation on Bone Healing of Ti_6Al_4V Alloy Implants in Rabbit Tibiae. *Biomaterials* **2007**, *28*, 3306−3313.

DOI: 10.1021/acsami.5b03209
ACS Appl. Mater. Interfaces 2015, 7, 13053−13061